Dye-sensitized solar cell module realized photovoltaic and photothermal highly efficient conversion via three-dimensional printing technology*

Qi-Zhang Huang(黄启章)[1,2], Yan-Qing Zhu(朱艳青)[1,2], Ji-Fu Shi(史继富)[1,3,†], Lei-Lei Wang(王雷雷)[1], Liu-Wen Zhong(钟柳文)[1], and Gang Xu(徐刚)[1,‡]

[1] *Key Laboratory of Renewable Energy, Guangzhou Institute of Energy Conversion, Chinese Academy of Sciences, Guangzhou* 510640, *China*
[2] *University of Chinese Academy of Sciences, Beijing* 100049, *China*
[3] *Department of Physics and Siyuan Laboratory, Jinan University, Guangzhou* 510632, *China*

(Received 9 October 2016; revised manuscript received 7 December 2016; published online 13 February 2017)

Three-dimensional (3D) printing technology is employed to improve the photovoltaic and photothermal conversion efficiency of dye-sensitized solar cell (DSC) module. The 3D-printed concentrator is optically designed and improves the photovoltaic efficiency of the DSC module from 5.48% to 7.03%. Additionally, with the 3D-printed microfluidic device serving as water cooling, the temperature of the DSC can be effectively controlled, which is beneficial for keeping a high photovoltaic conversion efficiency for DSC module. Moreover, the 3D-printed microfluidic device can realize photothermal conversion with an instantaneous photothermal efficiency of 42.1%. The integrated device realizes a total photovoltaic and photothermal conversion efficiency of 49% at the optimal working condition.

Keywords: 3D printing, dye-sensitized solar cell module, concentrator, microfluidic

PACS: 84.60.Jt, 88.40.–j, 88.40.F–, 88.40.hj **DOI:** 10.1088/1674-1056/26/3/038401

1. Introduction

The potential energy crisis and environmental pollution call for renewable energy as a substitute for the traditional fossil fuels. Among the renewable energy sources, solar energy is the cleanest and the most extensively available source. Thus, to harness the abundant solar energy in an environmentally friendly way, integrated photovoltaics of solar cells is a wise strategy.[1] Dye-sensitized solar cells (DSCs) have been considered as a promising candidate for large-area practical application due to their low cost, easy fabrication, and considerable efficiency.[2,3]

Yet, scaling up the DSCs (larger than 1 cm^2) will result in the growth of ohmic losses of the transparent conductive oxide (TCO), since the sheet-resistance ($R_s > 7\ \Omega{\cdot}sq^{-1}$) of TCO is not negligible in this case. Decline of the fill factor (FF) of the DSCs caused by the increase of ohmic losses needs to be taken into account and mitigated as well.[4] To meet the requirement of commercialization, breakthrough is still expected to further improve the power conversion efficiency (η) of DSCs. In order to reduce the ohmic loss and avoid the recession of photovoltaic performance, a grid electrode as a current collector is very helpful for the DSC module. However, the grid electrode for series or parallel connection must occupy a certain area of the DSC module, which wastes part of the solar radiation on the DSC module.[5] For silicon-based solar cells, the radiation loss caused by the grid electrode is only 3%–5% of the incident light, which has negligible effect on the efficiency of silicon-based solar cells.[6] By contrast, the radiation loss for the DSC module (about 20% of the efficiency) is very serious, though considerable width of the grid electrode (5–7 mm) is required to reduce series resistance.[7] Nevertheless, little attention is paid to the radiation loss for the DSC module caused by the grid electrode. If this loss is re-used effectively, it is definitely beneficial to the increase of the efficiency of the DSC module.

Moreover, in the real operating conditions, unlike the standard temperature of 25 °C, the increase of cell temperature due to the absorption of solar irradiation can negatively affect the power output of DSC module,[8] which is most likely attributed to the degradation of the dye,[9] volatility of the electrolyte,[10] improper sealing,[11] and back reaction.[12] Thus, cooling for the DSC module is equivalently necessary for their outdoor application.

Three-dimensional (3D) printing as a novel additive manufacturing technique can easily fabricate objects with complex geometries.[13] The 3D printer builds an object, layer by layer, based on a "sliced" 3D model constructed by a computer program, such as computer aided design (CAD).[14] There are

*Project supported by the National Natural Science Foundation of China (Grant Nos. 21103194, 51506205, and 21673243), the Science and Technology Planning Project of Guangdong Province, China (Grant Nos. 2014A010106018 and 2013A011401011), the Guangdong-Hong Kong Joint Innovation Project of Guangdong Province, China (Grant No. 2014B050505015), the Special Support Program of Guangdong Province, China (Grant No. 2014TQ01N610), the Director Innovation Foundation of Guangzhou Institute of Energy Conversion, China (Grant No. y307p81001), and the Solar Photothermal Advanced Materials Engineering Research Center Construction Project of Guangdong Province, China (Grant No. 2014B090904071).

†Corresponding author. E-mail: shijf@ms.giec.ac.cn
‡Corresponding author. E-mail: xugang@ms.giec.ac.cn

© 2017 Chinese Physical Society and IOP Publishing Ltd

three advantages of 3D printing technology over typical techniques like casting and lithography in reproducible manner. Firstly, 3D printing technology has the advantage of low-cost manufacture by saving the consumption of materials because printed materials can be relatively fully used and the need of a master for replica molding can be avoided.[15] Secondly, the flexibility for directly printing the as-required design files that can also be shared on line is simple to fulfill by the 3D printing technology. Thirdly, traditional techniques are hardly used to create complex structures like foam only by a one-step process while it is very convenient for 3D printing technology. Therefore, 3D printing technology has been broadly employed in manufacturing functional materials and devices including drug delivery platforms,[16] tissue scaffolds,[17] energy storage devices,[18] electrically conductive materials,[19] force-sensors, etc.[20] On the above bases, we look forward to the solution of the radiation loss and high temperature issues in DSC module through 3D printing technology.

In this paper, we first propose the preparation of a light concentrator and water cooling device using 3D printing technology, which respectively overcomes the problems of radiation loss and increased temperature for the DSC module. With the assistance of the 3D-printed concentrator, the efficiency of the DSC module can be improved. Besides, in addition to 3D-printed microfluidic device, the temperature of the concentrated DSC module can be cooled down so that the concentrated DSC modules can stably retain their considerably satisfactory performances. Moreover, the 3D-printed microfluidic device can additionally present a function for heat collector where the foam structure within the fluidic walls can minimize the thermal loss. The photovoltaic efficiency (6.9%) and photothermal efficiency (42.1%) in total add up to 49%, which is favorable for the industrialization of DSC module.

2. Experimental section

2.1. Preparation of DSC module

The DSC module is supplied by Yingkou OPV Tech New Energy Co., Ltd. Typically, 3 g commercial P25 powders (Degussa) and 3 g polyethylene glycol 600 (PEG) were added into anhydrous ethanol (5 ml) and ground in a mortar for 5 min. Then the mixture was put away to stand for 2 h and treated with ultrasonication. Part of the ethanol was removed by rotary evaporation to obtain viscous TiO_2 pastes. Fluorine-doped tin oxide glass (FTO, 7×9.3 cm^2, Wuhan Jingge solar technology Co.) was corroded by HCl and Zn powders and left with a grid area (10 rectangles, in total 17.4 cm^2) covered by plastic tapes (3M Co., Ltd.). The corroded FTO was ultrasonically cleaned by deionized water and ethanol. Silver grid lines were screen printed on the FTO surface using a 200 mesh screen and then dried at 180 °C for 10 min. The resulting TiO_2 pastes were used for the TiO_2 film on the left FTO by screen-printing technique, and then the film was dried for 15 min on a platform and sintered at 500 °C for 30 min. The obtained TiO_2 electrodes were treated in 40 mM aqueous $TiCl_4$ (Aladdin) at 70 °C for 30 min, washed with water and ethanol, and eventually immersed in an ethanol solution of cis-bis(isothiocyanato)bis(2,2'-bipyridyl-4,4'-dicarboxylato)-ruthenium(II)bis-tetrabutylammonium (N719 dye, 0.3 mM) for 12 h to obtain 17.4 cm^2 sensitized active area. Platinized counter electrodes were fabricated by using sputtering instruments. The sandwich-type solar cell was fabricated by overlapping the TiO_2 electrode with the platinized counter electrodes and sealed by a hot melt gasket that is 25 μm thick and made of the ionomer Surlyn 1702 (Dupont). The electrolyte was introduced into the cell via vacuum backfilling. The cell was placed in a small vacuum chamber to evacuate air from inside the cell. The electrolyte, which was composed of 0.03 M I_2, 0.06 M LiI, 0.6 M 1-butyl-3-methylimidazolium iodide, 0.1 M guanidinium thiocyanate, and 0.5 M 4-tert-butylpyridine in acetonitrile, was dripped on the holes in the back of the counter electrode. When exposing it again to ambient pressure, the electrolyte was driven into the cell. Finally, the hole was sealed using a hot-melt ionomer Surlyn and a cover glass (0.1 mm thickness). The obtained dye sensitized solar cell module is shown in Fig. 1(a).

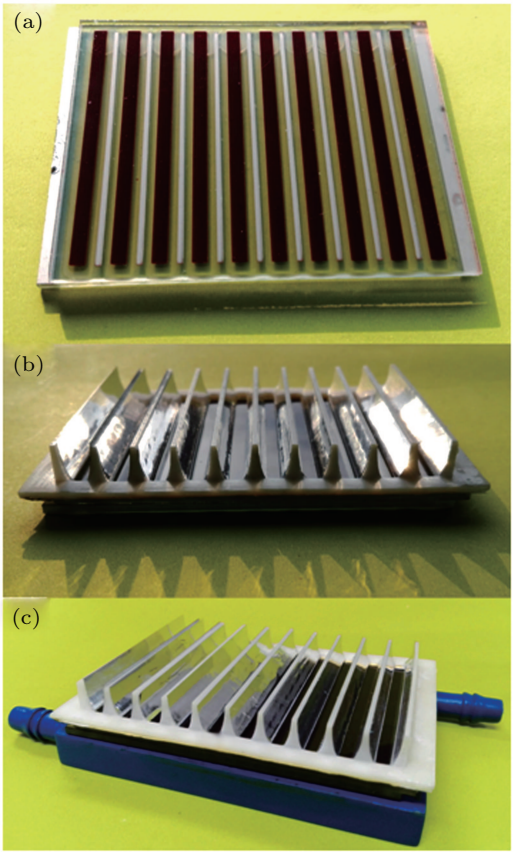


Fig. 1. (color online) Pictures of (a) DSC, (b) DSC with 3D-printed concentrator, and (c) DSC with 3D-printed concentrator and microfluidic device.

2.2. 3D-printed concentrator and microfluidic device

All 3D-printed devices were printed on an Objet Connex 350 printer. Designs of concentrator and microfluidic device were carried out by using TracePro and PTC Creo software, respectively. The structures were converted into STL files by Sketchup 2013 computer aided design (CAD) software. The material of 3D ink mainly contained polylactic acid (PLA). The printed concentrator and microfluidic device are opaque and rigid. The 10 parabolic troughs in the concentrator have been successfully printed in the microfluidic device. Mirror films were taped on the inwall of the parabolic troughs in the 3D-printed concentrator. The parabolic troughs fitted with the pattern of the DSC module were of 7 mm interval distance on the top and 3 mm at the bottom, where the geometric concentrating ratio is 7/3. The height of the parabolic troughs equals 7 mm. The digital photos of DSC module with 3D-printed concentrator are shown in Fig. 1(b). As shown in Fig. 2, the designed structure, printed product, and tunnels of the microfluidic device are presented. In Fig. 2(c), the microfluidic device accordingly has 10 channels which are 6 mm wide and 5 mm deep for water cooling. The total volume of the channels for water transport is 27 ml. To integrate the devices with micro-pump for water transport, two inlets were also printed for connection of silicone tubes. The digital photo of DSC module with 3D-printed concentrator and microfluidic device is presented in Fig. 1(c), where the concentrator is located above the module and the microfluidic device is well beneath it.

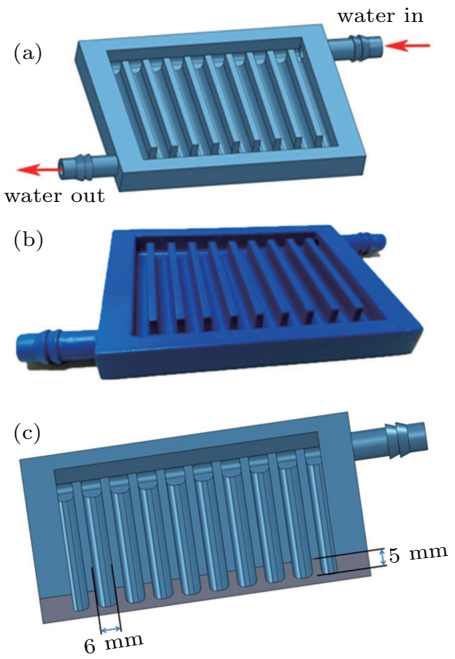


Fig. 2. (color online) (a) Structural illustration and (b) digital photo of the printed microfluidic device, and (c) architecture of microfluidic tunnels with cross-section.

2.3. Measurement

Photovoltaic conversion efficiency, short-circuit current, open-circuit voltage, and fill factor were evaluated by using a digital source-meter (Keithley 2400) and a 3A-class solar simulator (ABET: Sun 3000) which was corrected by standard silicon solar cell prior to test. The temperatures of the surface of DSC module and water in the microfluidic device were measured by temperature meter (TES1319).

3. Results and discussion

3.1. Optical design

The compound parabolic concentrator (CPC), which is very close to the ideal one and has a maximum theoretical concentration ratio, is used as the optical design of the 3D-printed concentrator. The CPC is designed by the edge-ray principle shown in Fig. 3. The PP′ and QQ′ are the entrance and exit apertures, the profile of the CPC between P′ and Q′ is of a parabola with axis parallel to PQ′ and with focus at Q. The equations of the profile of the reflective face are expressed in terms of the polar coordinates (r, φ) as follows:[21]

$$x = r\sin(\varphi-\theta_i)-a' = \frac{2f\sin(\varphi-\theta_i)}{1-\cos\varphi}-a' = \frac{2a'(1+\sin\theta_i)\sin(\varphi-\theta_i)}{1-\cos\varphi}-a', \quad (1)$$

$$z = r\cos(\varphi-\theta_i) = \frac{2a'(1+\sin\theta_i)\sin(\varphi-\theta_i)}{1-\cos\varphi}, \quad (2)$$

where a' is the half of the exit aperture, θ_i is the maximum acceptance angle with the concentrator axis, which is designed to be 12.5° in this paper.

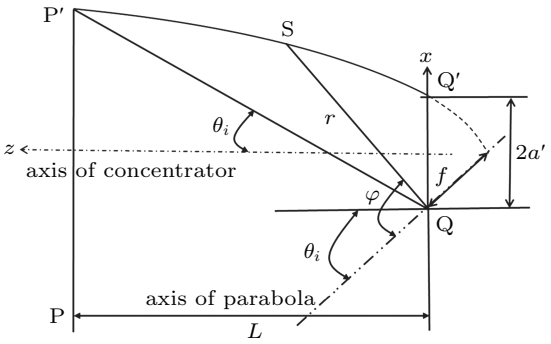


Fig. 3. Illustration of the constants in the equations of the profile.

By the Tracepro software, the solar ray paths in the 3D-printed concentrator and the focal spot distribution are simulated with 1000 incident rays at normal incidence, which are shown in Figs. 4(a)–4(c), respectively. Figure 4(b) shows the cross section of the ray paths in the concentrator at normal incidence, where the parallel rays are reflected by the parabolic

mirror in the concentrator and projected on the sensitized TiO_2 film. It can be seen in Fig. 4(c) that the focal solar rays distribute homogeneously on dye-sensitized TiO_2 film of the DSC. However, as is well known the construction of optical concentrator on solar cell may usually lead to non-uniform radiation projection and light shield at oblique incidence. Interestingly, with the help of ray tracing technique the optical losses can be eliminated in that case[22] implying that the 3D-printed concentrator has great potential application in solar tracking system with DSC module.

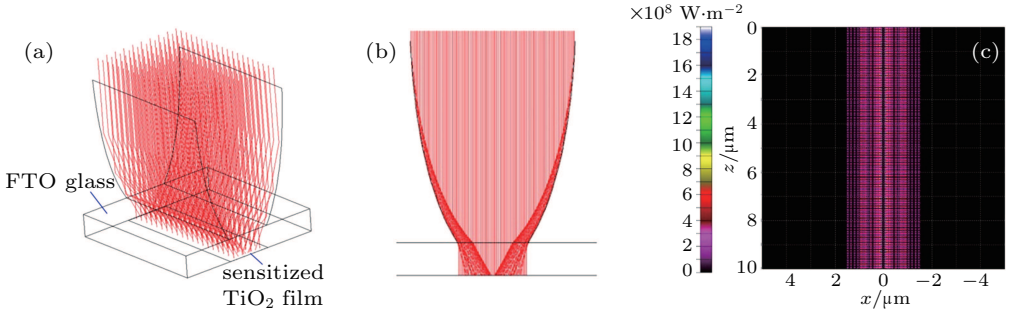


Fig. 4. (color online) (a) Diagram and (b) cross-section of ray-tracing, and (c) focal spot distribution map of 3D-printed concentrator.

3.2. 3D-printed concentrator applied in DSC module

The introduction of concentrator will result in an increase of the radiation on the unit area of the DSC module, thus it is important to observe the effects of irradiance on the J_{sc} and V_{oc}. The dependence of J_{sc} and V_{oc} on irradiance is shown in Fig. 5. It indicates that the J_{sc} increases linearly with the increase of irradiance, implying that electron recombination is not strongly affected by irradiance (as shown in Fig. 5(a)). Analogous phenomenon was also reported.[23] It also indicated that the light concentrator is feasible to effectively improve the efficiency. In addition, figure 5(b) displays the V_{oc} as a function of irradiance, showing that V_{oc} logarithmically increases with the increase of irradiance. The logarithmical relationship between V_{oc} and irradiance is modeled in the previous report.[24]

Furthermore, under a standard test condition (at 25 °C, under AM 1.5 simulated sunlight at a light intensity of 100 mW·cm^{-2}), the photocurrent density–voltage (J–V) curves of the DSC module (total area: 7×9.3 cm^2 and active area: 17.4 cm^2) without and with 3D printed concentrator are shown in Fig. 6. The short-circuit photocurrent density (J_{sc}), open-circuit voltage (V_{oc}), fill factor (FF), and overall conversion efficiency (η) of the DSC module without 3D-printed concentrator are 1.15 mA·cm^{-2}, 6.91 V, 0.7, and 5.48%, respectively. For the DSC module with 3D-printed concentrator, the photovoltaic parameters are 1.68 mA·cm^{-2}, 7.15 V, 0.63, and 7.03%, respectively. The lower FF of the DSC with 3D-printed concentrator than without concentrator may be attributed to the high concentration of the illumination which increases the resistive loss.[25] Regardless of the lower FF, the photovoltaic conversion efficiency ($\eta = 7.03\%$) of DSC with concentrator is still much higher, which is increased nearly by 30% of η (5.48%) of the DSC without concentrator. This result in general reveals that the 3D-printed concentrator improves the η of DSC due to its higher J_{sc} and V_{oc}. Meanwhile, single DSC with an active area of 0.16 cm^2 is also tested for comparison, which has V_{oc}, J_{sc}, FF, and η respectively equal to 0.76 V, 16.89 mA/cm^2, 0.67, and 8.6%. It indicates that series connection of single DSCs can enhance the V_{oc} due to potential accumulation but lower J_{sc} because of the electron recombination and increased series resistance.

In the outdoor application, DSC may suffer from high temperature because of the absorption of solar irradiation.

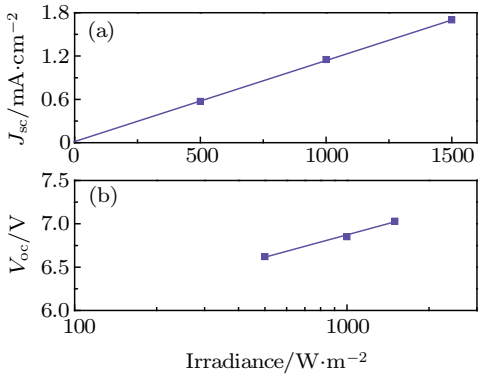


Fig. 5. (color online) Effects of irradiation on (a) short-circuit photocurrent density and (b) open-circuit voltage.

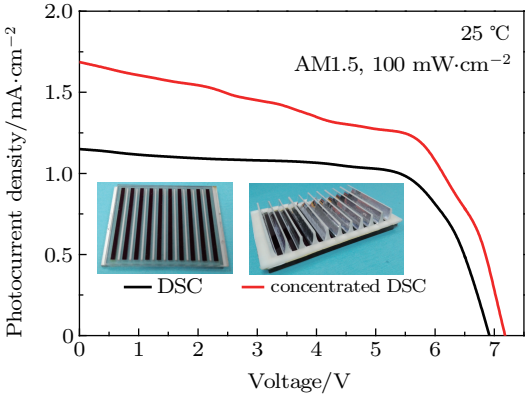


Fig. 6. (color online) J–V curves of DSC module without and with 3D-printed concentrator.

Thus, the photovoltaic parameters (J_{sc}, V_{oc}, FF, η) of DSC module with 3D-printed concentrator at temperatures from 10 to 55 °C under AM 1.5 at a light intensity of 100 mW·cm^{-1} are measured, and the results are shown in Fig. 7. It should be noticed that the variation trend of J_{sc} versus temperature strongly depends on DSC module feature such as the type of electrolyte, type of series interconnection, and type of sealant. For DSC with acetonitrile-based electrolyte, there is a strong influence of temperature on J_{sc} because mass transport in electrolyte is significantly affected by viscosity.[26] Besides, the appropriate sealing of DSC is essential for deterring the electrolyte from volatilizing and the low-boiling point electrolyte from leaking at high temperature (above 40 °C). Figure 7(a) shows two thermal regions of J_{sc} varying with temperature. When temperature is lower than 17 °C, J_{sc} increases fast with increasing temperature because of limitation of the diffusion of tri-iodide ions in the electrolyte dominates over the charge transport. Higher temperature makes the diffusion of tri-iodide ions easier due to the decrease of the viscosity. However, J_{sc} decreases slowly with temperature higher than about 17 °C. This change can be explained by the fact that higher temperature than $\sim$ 17 °C makes the rate of electron recombination much faster. Figure 7(b) shows the effect of temperature on V_{oc}. The V_{oc} decreases linearly with the increase of temperature due to the increased recombination probability. The linear dependence of V_{oc} on temperature has also been reported in other literature.[26,27] In Fig. 7(d), it indicates that η first increases and then decreases with increasing temperature. Now that the FF scarcely changes in a temperature range from 10 °C to 55 °C (see Fig. 7(c)), the change of η mainly results from the variations of J_{sc} and V_{oc}. In the first thermal region, the increased J_{sc} can compensate for the decrease of V_{oc} so that the η can increase. In contrast, the simultaneous decreases of J_{sc} and V_{oc} make η decrease in the second thermal region. This result implies that it is very significant to control the temperature to make the DSC module work near its optimal condition.

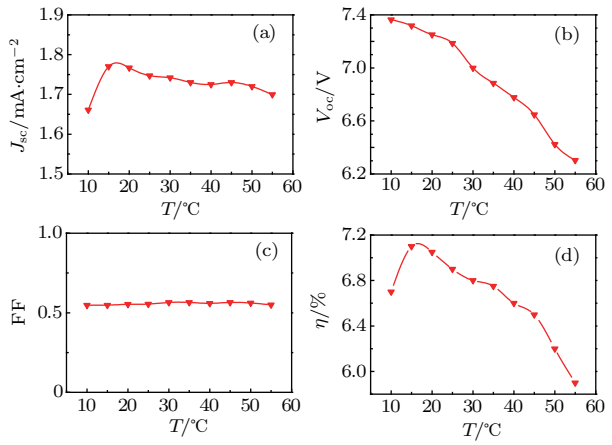


Fig. 7. (color online) Effects of temperature on (a) short-circuit photocurrent density, (b) open-circuit voltage, (c) fill factor, and (d) overall conversion efficiency.

3.3. 3D-printed microfluidic device applied in DSC module

From the above analysis, it should be noted that the temperature has a significant influence on the performance of DSC module. Hence, the temperature tests of the DSC module with 3D-printed concentrator under AM 1.5 simulated sunlight of 100 mW·cm^{-2} are evaluated, and the results are shown in Fig. 8. The temperature of the DSC with 3D-printed concentrator increases continuously during the exposure time within 25 min because the absorption of the solar light by the active area of the DSC module can produce not only electricity but also heat. However, the temperature tends to be a constant at about 52 °C after 25 min due to the thermal equilibrium between heat accumulation and heat emission. As can be seen in Fig. 7(d), the increased temperature negatively affects η of DSC module. Given this, the 3D-printed microfluidic device is used for water cooling of the DSC. In Fig. 8, with 3D-printed microfluidic device, the temperature of DSC tends to be invariant under AM 1.5 at 100 mW·cm^{-2} through the control of the water flow by a micro-pump. If the flow speed is further increased, the temperature of DSC can be more greatly reduced. This result indicates that a 3D-printed microfluidic device is beneficial for the cooling of the DSC module. Besides, the volatility of the solvent can be mitigated in this way so that the stability of the module is correspondingly improved if under air circumstance.

Meanwhile, the heated water can be considered as a photothermal application of the solar energy. The relationship between thermal efficiency (η_T) and $(T_bT_a)/I$ is determined as follows:

$$\eta_T = \frac{Cm(T_b - T_a)}{IAt}, \tag{3}$$

where C is the specific heat capacity of water, m is the mass of loading water, T_b is the outlet temperature, T_a is the inlet temperature, I is the intensity of solar irradiation, A is the effective area of DSC module (7×9.3 cm^2) normally facing the incident solar light, and t is time. The thermal performance of the collector can be evaluated by the curve of thermal efficiency versus the reduced temperature parameters $(T_bT_a)/I$ in Fig. 9, where the linear fitting is displayed as follows:[28]

$$\eta_T = 0.421 - 6.751\left(\frac{T_b - T_a}{I}\right).$$

The intercept of the equation corresponds to instantaneous thermal efficiency. The value of instantaneous thermal efficiency (42.1%) can be comparable to that of the recently reported photovoltaic/thermal system (40%).[29] The slope of the equation refers to heat loss coefficient (6.751 W/°C·m^2), which reflects the thermal insulation property of the system. The value of heat loss coefficient is lower than that of the recent reported thermal system (8.22 W/°C·m^2),[28] indicating that 3D-printed foam structure within the microfluidic device has considerable thermal insulation.

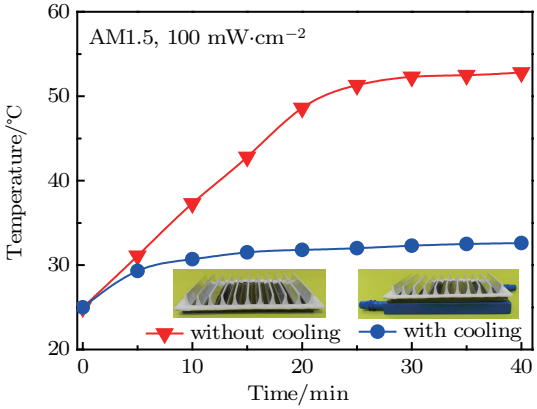


Fig. 8. (color online) Temperatures of DSC module without and with water cooling under AM 1.5 at 100 mW·cm^{-2}.

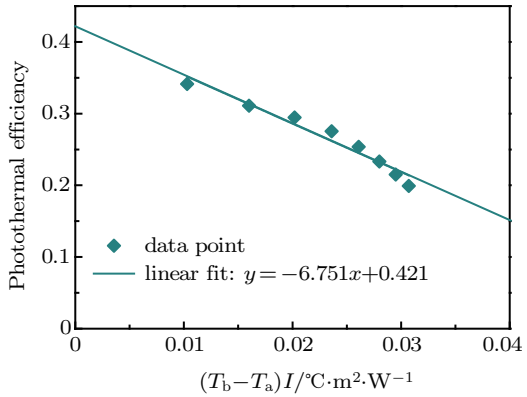


Fig. 9. (color online) Curve of the instantaneous thermal efficiency of the DSC module with 3D-printed microfluidic device.

In the DSC module with 3D-printed concentrator and microfluidic device, when the inlet temperature is 25 °C, the outlet temperature can reach 52 °C by a control of water flow at 0.7 ml/min, which is suitable for scouring bath (40–50 °C is recommended). At the water flow of 5.4 ml/min, the outlet temperature can be controlled at 32 °C. It indicates that the received hot water can be used for scouring bath, greenhouse cultural, and swimming pool (the temperature of ∼ 30 °C is recommended). In other words, the 3D-printed microfluidic device has a prosperous application in the above areas. However, the difference between inlet and outlet temperature is worthy of being noted, which may cause non-uniform temperature distribution and affect the performance of the DSC module. Although a cooling plate with excellent thermal conductivity is commonly used between the cell module and coolant to minimize the temperature non-uniformity,[30] temperature of different area in this module is detected during the testing at the water flow of 5.4 ml/min (with inlet and outlet temperature of 25 and 32 °C), revealing no obvious temperature gradient among the DSC units and sufficient thermal conductivity of FTO for temperature uniformity in this system. In contrast, if large temperature difference exists, a thermal conductor should be considered to be introduced between the cell module and water for temperature uniformity.

3.4. Energy harvest of DSC module with 3D-printed concentrator and microfluidics

In Fig. 10(a), for the DSC module with 3D-printed concentrator exposed to simulated solar irradiation (AM 1.5, 100 mW·cm^{-2}), the J_{sc} increases from 1.66 to 1.77 mA·cm^{-2} at the first 5 min due to the enhanced charge transport by high temperature. However, the slight decrease of J_{sc} within the next 25 min is ascribed to the increased electron combination at higher temperature. This consequence is in agreement with the result of Fig. 10(a) because temperature increases with exposure time. As shown in Fig. 10(b), due to the same reason, V_{oc} decreases from 7.3 to 6.3 V with time by increased temperature. Figure 10(c) shows the photovoltaic efficiencies of the DSC, the DSC with concentrator, and the DSC with concentrator and water cooling. Although the photovoltaic efficiency of the DSC with concentrator is higher than that of the DSC without concentrator, photovoltaic efficiencies of these DSC modules without and with concentrator exhibit the same variation trend, which is deteriorated as time goes due to effects of the vulnerable J_{sc} and the decay of V_{oc}. Thanks to the water cooling of 3D-printed microfluidic device, the photovoltaic efficiencies of DSC with concentrator can maintain at 6.9% with time, not affected by the increased temperature. This result also indicates a fact that 3D-printed microfluidic device as a water cooling section can improve the stability of the outdoor DSC module. The photothermal efficiency of the DSC with water cooling can be controlled at 42.1% with time, according to the intercept of the linear fit of instantaneous thermal efficiency. Consequently, the optimal total efficiency is equal to 49%, which is the summation of photothermal and photovoltaic efficiencies of the DSC module with concentrator and cooling. This total efficiency indicates that with the assistance of 3D-printed concentrator and microfluidic device, a relatively high solar energy conversion efficiency of 49% can be realized, which is about 9 folds of the efficiency of the DSC (5.5%). In Fig. 10(d), the received energy by different devices is recorded after an interval of every 10 min. The received energy can be continually accumulated with time. For the DSC module, the received energy is 5.68, 11.11, 16.23, and 21.14 kJ, respectively, corresponding to the time period of 10, 20, 30, and 40 min. For the DSC module with 3D-printed concentrator, the received energy increases from 7.12 kJ after 10 min to 26.67 kJ after 40 min. It can be noticed that the received energy of DSC module with 3D-printed concentrator and microfluidic device increases linearly with time due to its stable photovoltaic and photothermal efficiencies with time. After 40 min, the total energy (686.58 kJ) composed of the received energy from photovoltaic (28.81 kJ) and photothermal (657.77 kJ) conversion can be obtained.

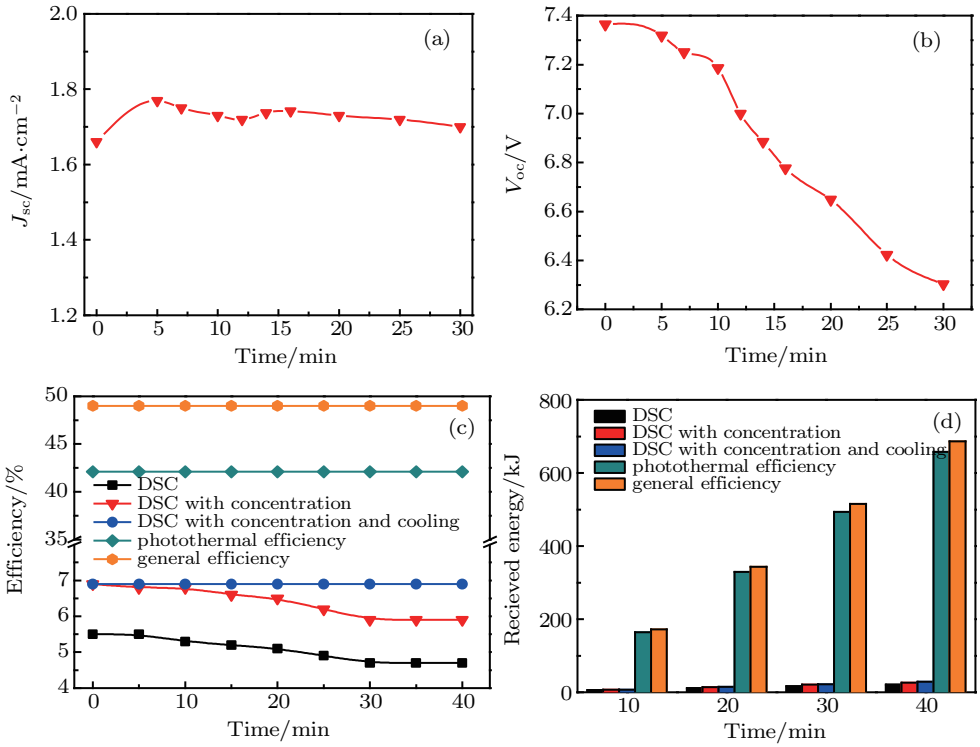


Fig. 10. (color online) Time dependence of (a) short-circuit photocurrent density, (b) open-circuit voltage, (c) energy efficiencies, and (d) received energy.

4. Conclusion and perspectives

A 3D-printed concentrator and microfluidic device are successfully applied in a DSC module whose active area is 17.4 cm^2. A 3D-printed concentrator can help to collect the sunlight projecting on the gap between the active areas and increase the photovoltaic efficiency of the DSC from 5.48% to 7.03%. On the other hand, a 3D-printed microfluidic device can function not only as water cooling for DSC to get rid of the negative effect from the increased temperature but also as a thermal collector for heating water, whose photothermal efficiency can reach 42.1%. Eventually, the integrated device with a favorable general efficiency of 49%, which is added up by the photovoltaic and photothermal efficiencies, realizes a high energy harvest of 686.58 kJ after working 40 min under AM 1.5 at light intensity of 100 mW·cm^{-2}. This technique exhibits a broad application prospect for outdoor DSC module.

References

[1] Sarsam W S, Kazi S N and Badarudin A 2015 *Solar Energy* **122** 1245
[2] Feng L F, Zhao K, Dai H T, Wang S G and Sun X W 2016 *Chin. Phys. B* **25** 037307
[3] Ma W, Zhang F and Meng S 2014 *Chin. Phys. B* **23** 086801
[4] Mariani P, Vesce L and Carlo A D 2015 *Semicond. Sci. Tech.* **30**
[5] Huang Y, Dai S Y, Chen S H, Hu L H, Kong F T, Kou D X and Jiang N Q 2010 *Acta Phys. Chim. Sin.* **59** 643
[6] Stuckings M F and Blakers A W 1999 *Sol. Energ. Mat. Sol. C* **59** 233
[7] Giordano F, Guidobaldi A, Petrolati E, Vesce L, Riccitelli R, Reale A, Brown T M and Carlo A D 2012 *Prog. Photovoltaics* **21** 1653
[8] Buhbut S, Clifford J N, Kosa M, Anderson A Y, Shalom M, Major D T, Palomares E and Zaban A 2013 *Energ. Environ. Sci.* **6** 3046
[9] O'regan B and Grätzel M 1991 *Nature* **353** 737
[10] Wang H, Xu X Q, Shi J F and Xu G 2013 *Acta Phys. Chim. Sin.* **29** 525
[11] Hagfeldt A, Boschloo G, Sun L, Kloo L and Pettersson H 2010 *Chem. Rev.* **110** 6595
[12] Dai P P, Yang L, Liang M, Dong H H, Wang P, Zhang C Y, Sun Z and Xue S 2015 *Acs Appl. Mater. Inter.* **7** 22436
[13] Yue J, Zhao P, Gerasimov J Y, Lagemaat M, Grotenhuis A, Rustema-Abbing M, Mei H C, Busscher H J, Herrmann A and Ren Y J 2015 *Adv. Funct. Mater.* **25** 6756
[14] Anderson K B, Lockwood S Y, Martin R S and Spence D M 2013 *Anal. Chem.* **85** 5623
[15] Gross B C, Erkal J L, Lockwood S Y, Chen C P and Spence D M 2014 *Anal. Chem.* **86** 3240
[16] Khaled S A, Burley J C, Alexander M R and Roberts C J 2014 *Int. J. Pharmaceut.* **461** 105
[17] Derby B 2012 *Science* **338** 921
[18] Sun K, Wei T S, Ahn B Y, Seo J Y, Dillon S J and Lewis J A 2013 *Adv. Mater.* **25** 4539
[19] Mannoor M S, Jiang Z, James T, Kong Y L, Malatesta K A, Soboyejo W O, Verma N, Gracias D H and McAlpine M C 2013 *Nano Lett.* **13** 2634
[20] Kim K, Zhu W, Qu X, Aaronson C, McCall W R, Chen S and Sirbuly D J 2014 *Acs Nano* **8** 9799
[21] Winston R 2005 *Nonimaging Optics* **264** 76
[22] Waghmare S A and Gulhane N P 2016 *Sol. Energy* **137** 165
[23] Huang S Y, Schlichthorl G, Nozik A J, Gratzel M and Frank A J 1997 *J. Phys. Chem. B* **101** 2576
[24] Snaith H J, Schmidt-Mende L, Gratzel M and Chiesa M 2006 *Phys. Rev. B* **74**
[25] Paul D I, Smyth M, Zacharopoulos A and Mondol J 2013 *Solar Energy* **33** 3
[26] Kuang D, Wang P, Ito S, Zakeeruddin S M and Graetzel M 2006 *J. Am. Chem. Soc.* **128** 7732
[27] Sebastian P J, Olea A, Campos J, Toledo J A and Gamboa S A 2004 *Sol. Energ. Mat. Sol. C.* **81** 349
[28] Zhu T T, Diao Y H, Zhao Y H and Li F F 2016 *Appl. Therm. Eng.* **98** 1201
[29] Zhao J F, Song Y C, Lam W H, Liu W G, Liu Y, Zhang Y and Wang D Y 2011 *Energ. Convers. Manage* **52** 1343
[30] Mittelman G, Kribus A and Dayan A 2007 *Energ. Convers. Manage* **48** 2483